

Four-terminal magneto-transport in graphene p-n junctions created by spatially selective doping

Timm Lohmann*, Klaus v. Klitzing, Jurgen H. Smet

Max-Planck-Institut für Festkörperforschung, Heisenbergstr. 1, 70569 Stuttgart, Germany

In this paper we describe a graphene p-n junction created by chemical doping. We find that chemical doping does not reduce mobility in contrast to top-gating. The preparation technique has been developed from systematic studies about influences on the initial doping of freshly prepared graphene. We investigated the removal of adsorbates by vacuum treatment, annealing and compensation doping using NH_3 . Hysteretic behavior is observed in the electric field effect due to dipolar adsorbates like water and NH_3 . Finally we demonstrate spatially selective doping of graphene using patterned PMMA. 4-terminal transport measurements of the p-n devices reveal edge channel mixing in the quantum hall regime. Quantized resistances of h/e^2 , $h/3e^2$ and $h/15e^2$ can be observed as expected from theory.

Since its discovery in 2004 (1) graphene, a single layer of hexagonally arranged carbon atoms, has developed into a fascinating material for research. Graphene's unusual band structure allows electric field tuning of both carrier type and concentration. The easily accessible surface offers unique possibilities for fabricating low dimensional systems. Chemical doping with gases has for instance been demonstrated in 2007 (2). With local gates

*t.lohmann@fkf.mpg.de

on top of graphene (3; 4) transport measurements in p-n junctions have been reported (5). Theoretical studies have predicted among others phenomena such as Klein tunneling (6) and Veselago lensing in ballistic p-n junctions (7).

Controlling the intrinsic doping as well as the capability to change the carrier density locally are very important issues for graphene devices. In previous works it has been shown that graphene is extremely sensitive to molecular adsorbates (2) and top gates have been used to control the carrier density in selected areas of the sample (3; 4). The tuning capability of a top-gated p-n junction goes at the expense of reduced sample quality. The mobility drops due to the presence of the top-gate oxide. Here we demonstrate a different technique based on chemical doping to change the carrier density in selected areas of the graphene samples. As we show later chemical doping does not reduce the sample's mobility if executed at room-temperature. Initially, we investigated the influence of molecular adsorbates on the field effect behavior of graphene to gain a better understanding on how to manipulate the adsorbates. For spatial control resist masks have been used which can be easily patterned with e-beam lithography. Parts of a graphene sample are covered by the resist while the uncovered parts can be exposed to dopants like NH_3 . This technique allows us to create carrier density steps and hence provides an alternative route to fabricate p-n junctions. The overall density can be tuned with the help of a global back-gate. The electronic transport properties of these p-n devices were investigated in a four terminal geometry as a function of the magnetic field and carrier density. In the quantum Hall regime, our measurements yield evidence for edge channel equilibration similar to what has been demonstrated in a two terminal geometry (5).

Individual graphene flakes were prepared on highly n-type doped Si-substrates with a 300 nm thick thermally grown SiO_2 layer at the top using a micromechanical cleavage method, similar to the one described in Ref. (1). Monolayers were identified with the help of optical microscopy (8) and Raman spectroscopy (9). Cr/Au (3nm/30nm) contacts were patterned via electron beam lithography. The global density of the sample can be changed

by applying a voltage to the backside of the doped Si-substrate. Four-terminal resistance measurements were performed in a Hall bar configuration with a sinusoidal source-drain current of 100 nA. A typical contact geometry used to explore spatially selective chemical doping is shown in 1. The present paragraph focuses on similarly contacted graphene samples but without partial PMMA (Polymethylmethacrylate) coverage. The sample was

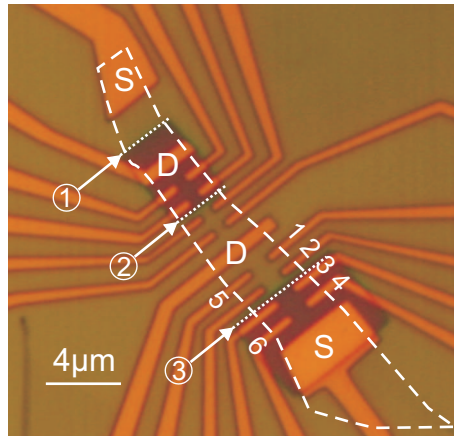


Figure 1: A contacted graphene mono layer with a patterned layer of PMMA on top. The white dashed line highlights the edges of the graphene flake. Two windows in the PMMA allow to selectively dope the flake underneath in these regions. This procedure results in three independent p-n junctions (numbers in circles) for this particular design. Contacts used as source (S), drain (D) and voltage probes (1 to 6) are labeled.

mounted in a sample stick with the following capabilities: (i) The sample space can be evacuated down to 10^{-5} mbar. (ii) Gases such as NH_3 , Ar, He and O_2 can be introduced in a controlled fashion. (iii) The sample can be heated up to 420 K. In addition, it is possible after heat or gas treatment to transfer the sample into helium atmosphere and cool it down to 1.5 K without any exposure to air. The resulting experimental set-up can be used to chemically dope the flake, control the value of the doping concentration in situ at room temperature (RT) and subsequently freeze it in the cryostat to carry out low temperature transport studies in magnetic fields up to 12 T.

Our studies first address the room temperature field effect characteristics on freshly prepared flakes under ambient conditions. The four terminal sample resistance exhibits strong

hysteretic behavior. When comparing up and down sweeps of the back-gate voltage the resistance reaches a maximum at different back-gate voltages for the two sweep directions as illustrated in 2a. The peaks are shifted by as much as 10 V which corresponds to a density difference of $0.8 \cdot 10^{12} \text{ cm}^{-2}$. For samples with higher initial doping the hysteresis or splitting is even larger (for instance 3a, dotted curve). The observed behavior is known from carbon nanotubes (10) and was attributed to dipolar adsorbates such as water which act as charge traps. When executing subsequent up and down sweeps, small deviations from the first cycle are observed. The splitting however stays constant. This has been verified for up to 10 cycles. Since charge trapping by water is a dynamic process it depends on the sweep conditions of the applied gate voltage. Low sweep rates result in a large splitting of the resistance peaks as shown in 2b. We display curves for two different values of the sweep rate: 0.25 V/s and 1.75 V/s. A second relevant parameter is the sweep interval, i.e. the amount of charge injected into the sample. A large voltage span such as [-70V, 70V] produces a large splitting. 2c displays data recorded for two gate-voltage sweeps: from -70 to 70 V and -20 to 20 V. Other sweep conditions yield a consistent dependence as shown in 2d.

In order to influence the sample's initial doping and the hysteresis described above we treated samples under various conditions. The three important parameters, which were explored, are (i) vacuum down to 10^{-5} mbar, (ii) temperatures of about 420 K and (iii) gas atmosphere in the sample chamber. Changes in the sample quality and doping by varying these parameters were assessed by investigating the following sample characteristics: (1) The existence of hysteresis in the field effect behavior, which can be caused by the presence of dipolar species. (2) The back-gate voltage at which charge neutrality is achieved. It serves as an indicator for the amount of (unintentional) doping. (3) The resistance/conductance at the charge neutrality point. It reflects the degree of density inhomogeneity in the sample. (4) Finally, the mobility difference between Dirac electrons and holes. It is governed by the type and number of doping adsorbates. In the following paragraphs, we will discuss how

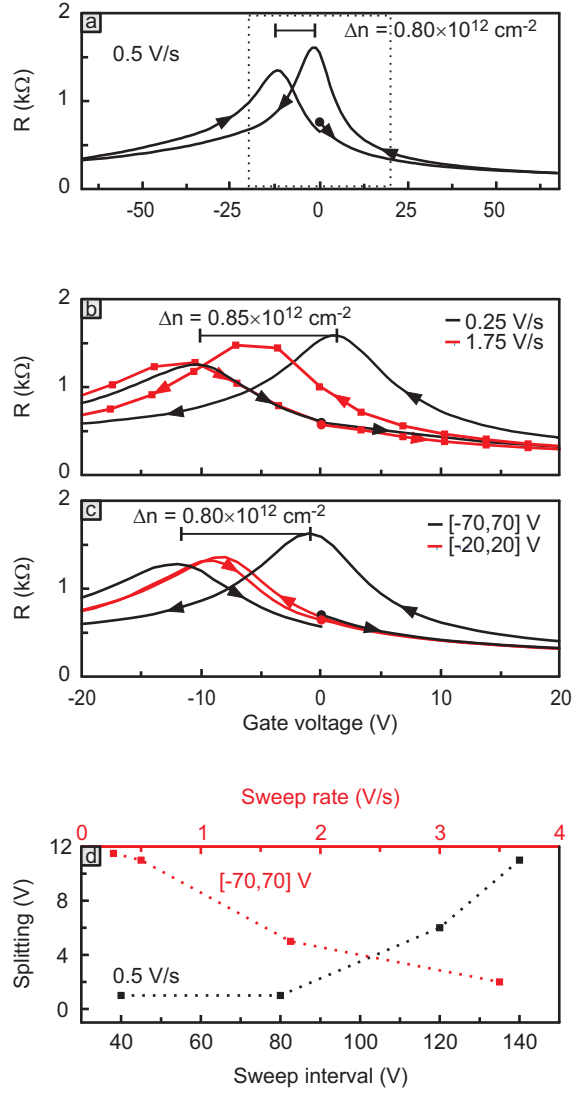


Figure 2: (a) Hysteresis in the field effect behavior of a low doped graphene monolayer under ambient conditions. The measurement was recorded by starting from zero back-gate voltage (black-dot), sweeping to +70 V, then -70 V and back to zero. The hysteresis is attributed to dipolar adsorbates such as H₂O. The arrows indicate the sweep direction. The measurement was executed at a sweep rate of 0.5 V/s. The dotted rectangle marks the gate voltage span plotted in panels b and c. (b) Field effect hysteresis for two different gate voltage sweep rates: 0.25 V/s and 1.75 V/s. The gate voltage is swept in the range of [-70, 70] V. (c) The same measurement as in b but here the voltage span serves as the parameter: [-20, 20] V and [-70, 70] V. The sweep rate is equal to 0.5 V/s. (d) Splitting as a function of the voltage interval (bottom x-axis in black) and sweep rate (top x-axis in red). The red/black dotted lines are guides to the eye.

each of these characteristics change.

Vacuum treatment: Keeping a freshly prepared sample under $3 \cdot 10^{-5}$ mbar at room temperature for several hours strongly changes the field effect behavior. It diminishes the hysteresis and frequently also causes a shift of the charge neutrality point closer to zero back-gate voltage. An example is shown in 3a. The hysteresis has nearly vanished after pumping down to $3 \cdot 10^{-5}$ mbar for 15 hours (black curve). The charge neutrality point lies in between the peaks of the up and down sweep recorded prior to sample evacuation (black dotted line for comparison). After continued pumping for a total of 50 hours (blue curve) a significant shift of the charge neutrality point is observed. Presumably, this shift is caused by the gradual desorption of doping adsorbates in vacuum. Since no elevated temperatures are required to induce a change, it indicates that at least one adsorbed species that causes hysteresis and p-doping is only loosely bond to the graphene surface. The desorption is also accompanied by an increase of the resistance at the charge neutrality point from $\approx 2 \text{ k}\Omega$ to $\approx 3 \text{ k}\Omega$. The non-zero conductivity at charge neutrality likely originates from the existence of electron and hole puddles as demonstrated in scanning SET (single electron transistor) experiments (11). Even though on average the sample is charge neutral, locally charge carriers are available and Klein tunneling ensures that transport across puddles of opposite charge polarity is not impeded. The increase of the resistance at the charge neutrality point suggests that fewer charge carriers are available in the electron and hole puddles because of a reduced amplitude of the density fluctuations. Finally, note that the blue curve after 50 hours of vacuum treatment exhibits a pronounced asymmetry between the electron and hole conduction (blue circles mark two voltages where the electron and hole density are equal). These observations will be discussed in more detail below.

Sample annealing: Heat treatment is the second possibility to remove dopants. It is more effective than pumping and requires less time. Heat treatment improves the sample quality in terms of our four criteria: smaller hysteresis, a charge neutrality point closer to zero back-gate voltage, a larger resistance at the charge neutrality point and a smaller mobility

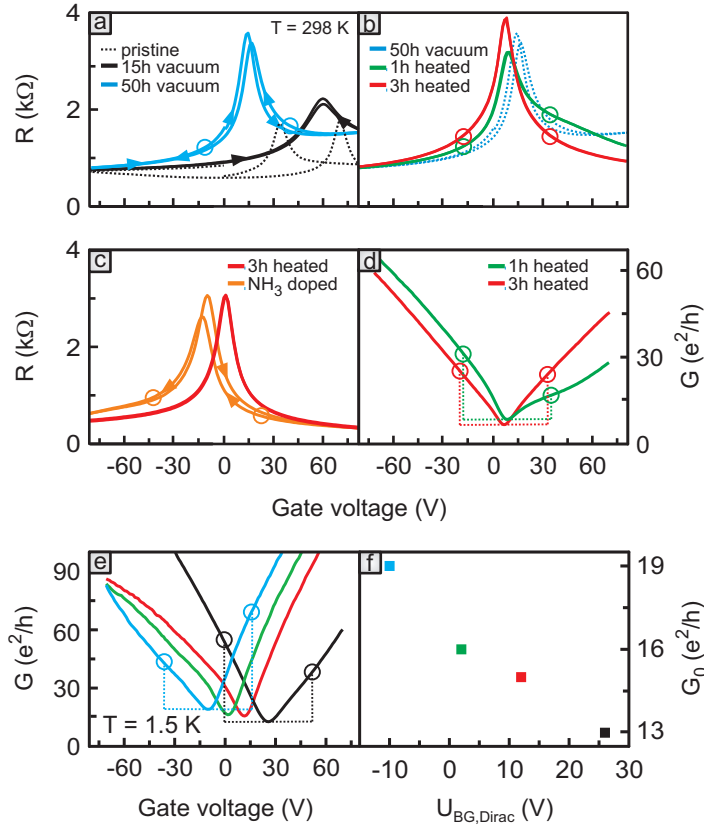


Figure 3: (a) Vanishing hysteresis after 15 hours in vacuum at $3 \cdot 10^{-5}$ mbar (black curve) for a highly doped sample. Reduced intrinsic doping and hysteresis after 50 hours in vacuum (blue curve). The black dotted line shows the initial state of the sample after preparation. (b) Field effect behavior after 1 hour (green curve) and 3 hours (red curve) annealing at 420 K and 10^{-5} mbar. The blue dotted line is the curve from (a) after 50 hours in vacuum. (c) Shifting the charge neutral point by chemical doping using NH_3 . The initial curve (red) is measured after 3 h annealing. A hysteresis appears due to the dipolar nature of NH_3 (similar to that caused by water but with opposite direction). (d) Conductance plot of the green and red curve from 3b to bring out better the difference between electron and hole conduction. All measurements in (a) to (d) were performed at ≈ 298 K. (e) Influence of doping on the e-h asymmetry. The black curve shows the conductance of a freshly prepared sample at 1.5 K. The red, green and blue curve are measured successively after an extra dose of 0.1 mmol NH_3 was introduced into the sample chamber at room temperature. One hour after each additional gas exposure, the sample was cooled back down to 1.5 K for the measurement in order to freeze out the hysteresis. The equidistant shift of ≈ 12 V to the left between the curves confirms that NH_3 compensates the initial p-doping. Note that the asymmetry between electron and hole conduction is inverted upon doping with NH_3 (compare the black and blue circles). (f) Plot of the conductance G_0 at the charge neutral point taken from the data in panel e versus $U_{BG,Dirac}$.

difference between electrons and holes. This is in agreement with previous reports (see Moser et al. (12), Ishigami et al. (13)). We note that heating should proceed under vacuum conditions, but a long term initial pumping is not needed to reach the end result. Pumping alone might be useful for devices which should not be exposed to elevated temperatures. Here we illustrate how the sample that underwent the 50 hour evacuation reacted to the heat treatment (3b). The hysteresis has vanished entirely after the anneal. The charge neutrality point has not shifted much further. The difference between the electron and hole mobility remains present after a 1 hour anneal (green circles), but has disappeared after 3 hours of annealing (the red circles have no vertical offset). The resistance at the charge neutrality point slightly dropped after 1 hour of heat treatment, but increased to about $4\text{ k}\Omega$ after a 3 h anneal at 420 K in vacuum. These observations all suggest that most of the initially adsorbed species are removed after annealing. (i) When dipolar adsorbates are effectively removed during the anneal, the hysteresis will vanish. (ii) When p-dopants such as water and oxygen disappear during the anneal, the charge neutrality point will shift close to zero back-gate voltage. (iii) The amplitude of the density fluctuations in the sample may drop upon removal of doping adsorbates. It will increase the resistance at the charge neutrality point.

Gas exposure: The amount of doping can of course also be manipulated by exposing the sample to suitable gases. In 3c we illustrate doping with NH_3 . The red curve has been measured on a sample similar to the one described previously after a 3 hour anneal. NH_3 acts as an n-type dopant and indeed the charge neutrality point shifts to negative back-gate voltages (orange curve) after the flake has been exposed. Hence, part of the initial p-doping is compensated. Note that a small hysteresis reappears with opposite sign as in 2. It is attributed to the dipolar nature of the NH_3 molecules. An asymmetry between the electron and hole side is also clearly visible in the orange curve (orange dots), but it is distinct from the asymmetry observed on flakes that were not treated with NH_3 in 3a and b. Untreated flakes exhibit superior hole conduction, while the NH_3 treated case shows better

electron than hole conduction. 3e illustrates the evolution of the field effect behavior when gradually exposing a flake to a larger amount of NH_3 . The black solid line represents the conductance obtained on the as prepared flake at 1.5 K. The sample was then warmed up in vacuum to room temperature and exposed to a dose of 0.1 mmol of NH_3 . After cooling back down to 1.5 K, the field effect behavior was recorded again. The same procedure was repeated several times. For each additional gas exposure the charge neutrality point shifted by approximately -12 V confirming that NH_3 molecules act as n-type dopants. The conductance at the charge neutrality point increases with increasing gas exposure. It is plotted in panel f as a function of the back-gate voltage at which charge neutrality is reached. These data suggest that spatial density fluctuations are enhanced upon doping, which would imply that the NH_3 molecules get preferentially adsorbed in certain regions only and not homogeneously across the entire flake. This issue may be intimately connected with the memory effect observed when flakes, which were treated in vacuum are exposed back to air. As we showed above, the vacuum and heat treatment drastically changes the four characteristics. They however return to their initial values (within a tolerance of a few % only) after a short time (< 1 min) when exposing the flake back to air irrespective of the duration and sequence of treatments. This reversibility adds support to the argument that doping adsorbates preferentially attach to surface and edge specific locations of the pristine flake. A similar argument was invoked previously in Ref. (14). A theoretical description of how dopants may affect the conductance at the charge neutrality point has been reported by Cheianov et al. (15) and is based on percolation in a random network of resistors.

The experiment with gas exposure in 3e also convincingly demonstrates the polarity dependent impact of doping adsorbates on the mobility of charge carriers. For the as prepared flake with substantial initial p-doping due to water and oxygen for instance, hole conduction excels over electron conduction when comparing the conductance values for identical electron and hole densities. The same was already seen in panels a-d (in particular panel d, where the resistance data of panel b is replotted on a conductance axis). However,

upon exposing the flake to more and more NH_3 , electron conduction becomes superior. The conductance at identical carrier densities is highlighted for one particular density with circles for some curves in the different panels to ease the comparison. The development of this asymmetry between the electron and hole side is in qualitative agreement with recent theoretical work (16). It was attributed to the energy dependent scattering potential generated by molecular adsorbates. The scattering potential suppresses conductance on one side of the Dirac point depending on the n- or p-type character of the doping adsorbate, while for the other side conductance is only weakly influenced. The deposition of metallic contacts has also been held responsible for the appearance of an electron-hole asymmetry in Ref. (17). These authors have invoked charge-density pinning underneath contacts to explain this asymmetry. Scanning photocurrent microscopy experiments (18) have indeed verified that deposited metals cause a doping of graphene and a density pinning in the vicinity of contacts. This doping in turn may be a cause of the observed asymmetry in Ref. (17). The sign of the asymmetry observed in our experiments for p- and n-doping is consistent with the I-V measurements for p- (Au) and n-doping (Ti) metals in Lee et al. (18). Note that the removal of adsorbates upon vacuum and heat treatment largely removes the mobility difference between electrons and holes (3b and c, red curves for instance) as anticipated for ideal graphene in view of the intimate connection between Dirac electrons and holes. Although the asymmetry can be removed we do not observe a significantly increasing mobility after annealing. The mobilities of our freshly prepared samples lie between 5000 and 8000 cm^2/Vs . Under the PMMA we have mobilities between 3000 and 5000 cm^2/Vs .

In the following section we demonstrate that chemical doping can be exploited to study graphene p-n junctions when masking part of the graphene layer with a resist. In a first step, ohmic contacts are made to a graphene monolayer using electron beam lithography. Subsequently, the sample is coated with a PMMA resist layer of 200 nm thickness. A second electron beam lithography step opens windows in this resist layer. The sample is

then mounted in the sample holder with vacuum chamber. Exposure to any gas, which dopes either n - or p -type, creates a density step at each boundary between the exposed graphene and those regions of the graphene flake still covered by PMMA. 1, discussed briefly previously, shows an optical image of such a flake with two windows in the PMMA layer on top. The flake itself is demarcated by the white dashed line. This device contains three such p-n junctions (dotted lines), which are labeled with the encircled numbers. Junction 1 makes up a two terminal geometry, while the others can be measured in a four terminal configuration. All data shown in this section have been acquired using the voltage probes 1 through 6 of junction 3. The two other devices revealed similar behavior.

After mounting the sample in the sample holder with vacuum chamber, it was annealed in vacuum at 420 K in order to remove residual adsorbates on those parts of the flake not covered by resist. The sample chamber evacuation and the heat treatment already introduce a doping step across the flake, since adsorbates underneath the PMMA can either not be removed or diffuse only slowly. The carrier density of the covered and uncovered areas can be monitored in situ by measuring the resistance in both regions as a function of the back-gate voltage during pumping and annealing in vacuum at room temperature. After this procedure the sample is transferred into the cryostat without exposure to air. 4 displays such field effect measurements for the PMMA covered (black line, voltage probes 1 and 2) and the exposed part of the graphene flake (red line, voltage probes 3 and 4) after evacuation and annealing. The charge neutrality points are reached at back-gate voltages of $V_{\text{Dirac}}^{\text{covered}} = 32 \text{ V}$ and $V_{\text{Dirac}}^{\text{uncovered}} = 9 \text{ V}$. For the sake of completeness we also show the longitudinal resistance measured across the junction (green line, voltage probes 2 and 3). The difference in the charge neutrality points corresponds to a density difference of $1.8 \cdot 10^{12} \text{ cm}^{-2}$. By choosing a back-gate voltage in between (19 V) a p-n junction is created. The inset in 4 depicts the $I-V$ characteristic measured between the source and drain contact across the p-n interface, which forms at a back-gate voltage $V_{\text{bg}} = 19 \text{ V}$. The measurements were carried out at 1.5 K. The $I - V$ trace does not resemble that of a conventional p-n

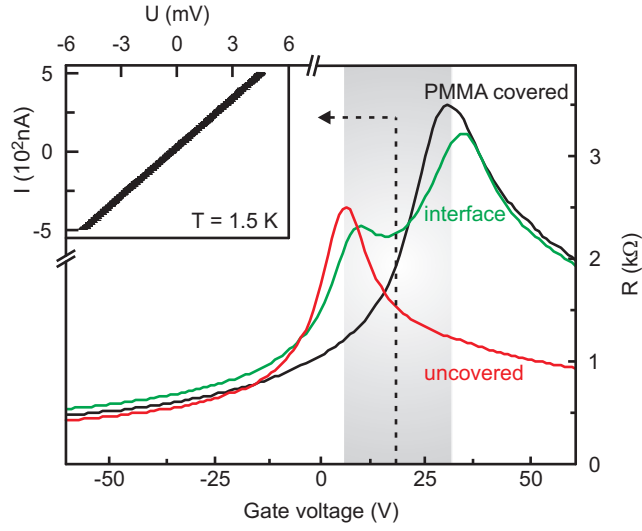


Figure 4: Field-effect measurement of a device as shown in 1. The black and red curves display the field-effect behavior in the PMMA-covered and uncovered regions. The two regions exhibit a density difference of about $1.8 \cdot 10^{12} \text{ cm}^{-2}$. The green curve was recorded across the interface of the two regions and is a superposition of the black and red curves. By choosing a back gate voltage in between the charge neutrality points of both regions a p-n junction is formed. The p-n region has been highlighted with a gray shading. The inset shows the I-V characteristics of such a p-n interface for a backgate voltage of 19 V. As theoretically predicted (6) the device shows no "diode-like" behavior but rather Ohm's law.

diode in accordance with theory (6). In a conventional semiconductor charge carriers have to overcome a bandgap in order to reach the conduction band. Therefore a conventional p-n junction is a diode in contrast to that in gapless graphene. But the missing gap is not the only reason for the absence of a diode-like I-V curve in graphene. A deeper reason is the conservation of the pseudospin which acts as an additional quantum number. It is a consequence of graphene's unusual bandstructure. Pseudospin conservation allows charge carriers in graphene to tunnel through a potential barrier like a p-n interface with 100% efficiency at normal incidence, independent of the width and height of the barrier. A gapless material with a parabolic bandstructure would show an oscillating transmission coefficient between zero and one while that of graphene is always one.

Therefore the measured $I - V$ characteristic is ohmic with a resistance of $9 \text{ k}\Omega$. The device geometry has approximately 1.5 squares. In view of the two terminal configuration, this resistance still contains contributions from the metal contact-graphene interfaces. From a comparison with four-terminal resistance measurements, we estimated the contact resistance to be below $1 \text{ k}\Omega$.

The graphene p-n junctions fabricated by spatially selective chemical doping were investigated further in the quantum Hall regime. In graphene one expects an unconventional integer quantum Hall effect (19; 20) due to the presence of a Landau level at zero energy (Dirac point), which is shared by both electrons and holes. Each Landau level is four fold degenerate due to the valley and spin degree of freedom. Therefore, when the spin and valley degeneracies are not lifted the system condenses in integer quantum Hall states when the filling factor ν , i.e. the number of filled Landau levels, equals $2, 6, 10, \dots$ and $-2, -6, -10, \dots$ with Hall resistance $R_{xy} = h/(e^2\nu)$. Negative filling factors correspond to hole fillings. In order to avoid parasitic effects from folded/misshaped edges we use graphene devices patterned into a Hall bar shape with e-beam lithography and oxygen plasma etching for these experiments. Furthermore the Hall bar geometry has the advantage that the metal/graphene interfaces of the contacts can be far away from the measured region. The

reported doping due to metal deposition (18) has then no influence for a measurement of the longitudinal resistance itself. The PMMA masking and contact scheme is similar to the device shown in 1. 5a shows the Hall resistance R_{xy} of two separate regions with different densities n_1 and n_2 . The shift between the charge neutrality points, i.e. the resistance maxima, of about $15 V$ corresponds to a density difference $\Delta n = |n_2 - n_1| = 1.2 \cdot 10^{12} \text{ cm}^{-2}$. This value is not arbitrary but was chosen carefully in order to ensure that the two regions with different density simultaneously condense in distinct integer quantum Hall states. The following combinations of integer filling factors (ν_1, ν_2) can be reached (see 5a) as the back-gate voltage is swept: (10,6), (6,2), (2,-2), (-2,-6) and (-6,-10). Hence p^+p , nn^+ as well as p - n junctions can be formed.

When the p - and n -regions condense in a quantum Hall state, the bulk turns incompressible and chiral edge channels flow along the boundary in opposite directions for the p and n -regions. Previous experimental work on two-terminal p - n junctions in a strong perpendicular magnetic field has shown that under quantum Hall conditions for both the p and n -region edge channels equilibrate efficiently when they meet at the p - n interface (5). It gives rise to two terminal resistances, which are properly predicted within the Landauer-Büttiker edge channel picture under the assumption of full equilibration (21). While these previous studies focused on two terminal devices, here we address this physics in the four terminal configuration. Apart from removing the contact resistance contribution, a four terminal arrangement offers the advantage that one can measure voltage drops across the junction before and after edge channels interacted on the opposite boundaries of the sample as schematically depicted in 5e. For the p - n regime, the Landauer-Büttiker formalism predicts

$$R_b = \frac{h}{e^2} \left(\frac{1}{|\nu_1|} + \frac{1}{|\nu_2|} \right) \quad \text{and} \quad R_a = 0 \quad (1)$$

before (R_b) and **after** (R_a) edge channels interact along the junction. If the carrier type

is the same on either side of the junction, these resistances read

$$R_b = 0 \quad \text{and} \quad R_a = \frac{h}{e^2} \left(\frac{1}{|\nu_1|} - \frac{1}{|\nu_2|} \right) \quad (2)$$

for the p^+p or nn^+ -regime. ν_1 and ν_2 are the filling factors in the adjacent regions of the sample. If in both regions the charge carriers possess the same polarity, edge channels do not interact along the junction itself, but rather when those originating from the region with a lower absolute filling factor have crossed the junction (right panel of 5e). The above description assumes full equilibration of the electrochemical potentials of the edge channels where they interact. As illustrated in the lower row of panels in 5e, inverting the direction of the magnetic field interchanges the Hall bar side where the interaction of edge channels did not take place yet with the Hall bar side where edge channels have interacted. The formulas for R_b and R_a remain unaffected. Note that measuring the longitudinal resistance on opposite sides of the Hall bar is equivalent to inverting the sign of the magnetic field.

A color rendition of the longitudinal resistance R_{xx} as a function of the magnetic field and the back-gate voltage is shown in 5b. These data allow us to verify the above picture. A hallmark of a four terminal Quantum Hall effect (QHE) experiment on a sample with regions of different filling factors is the magnetic field-asymmetry of R_{xx} . In a graphene device without a junction, the measurement of R_{xx} would yield a magnetic field-symmetric Shubnikov-de Haas fan since there is no distinction between the resistances measured on opposite sides of the sample. In the p-n junction here, which forms for back-gate voltages between -5 and -25 V, one observes zero resistance for fields between 8 to 12 T, while a resistance of approximately 25.5 k Ω is recorded at negative fields -8 to -12 T (or equivalently on the opposite edge of the sample). These two cases correspond to the top and bottom left panels in 5e when measuring the resistance across the junction using voltage probes at the bottom of the Hall bar geometry. In the top left panel for positive values of the magnetic field, the edge channels originating from the source and drain contact have equilibrated their electrochemical potentials as they are jointly running along the junction. There is

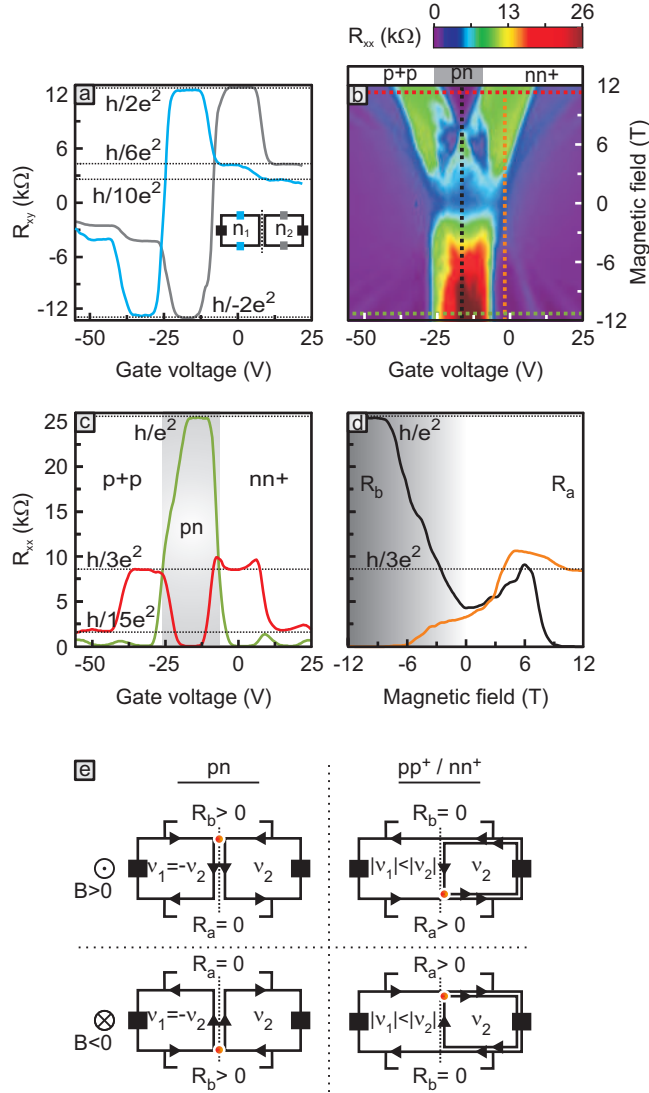


Figure 5: Low temperature (1.5 K) magneto transport behavior of a graphene p-n junction created by selective chemical doping. (a) Hall resistance R_{xy} in two regions with different doping measured as a function of the gate voltage. The magnetic field is 12 T. The doping difference of about 15 V ($1.2 \cdot 10^{12} \text{ cm}^{-2}$) provides a precise overlap of neighboring filling factors. The drawing illustrates the device geometry. (b) Color rendition of the longitudinal resistance R_{xx} as a function of the magnetic field and the gate voltage. The dotted lines belong to 5c,d. (c) Plot of the horizontal line sections from 5b. The characteristic resistance quanta h/e^2 , $h/3e^2$ and $h/15e^2$ are indicated by black dotted lines. (d) Plot of the vertical line sections from 5b. The grey/white region highlights the regime before/after edge channel interaction. (e) Schematic of edge channel mixing in 4-terminal geometry for the bipolar (p-n) and homopolar (p+p/nn+) case and for positive and negative magnetic field. The orange dots show where edge channel equilibration most likely takes place in the two cases.

no longer a difference in the electrochemical potentials when measuring at the bottom. The recorded resistance is zero. For negative values of the magnetic field, edge channel potentials are probed prior to equilibration along the p-n interface. Hence, the resistance is determined by the potential difference applied across the source and drain contacts. Since $\nu_1 = -2$ and $\nu_2 = 2$ we anticipate $R_b = h/e^2$ (Eq. 1) or 25812.807Ω . Our measured value of $25.5 \text{ k}\Omega$ is within the precision of our experimental setup.

When the system condenses either in a combination of the (-6,-2) or (2,6) integer quantum Hall states, the resistance drops to zero in both cases. This is again in line with the above edge channel picture. As seen in the bottom right panel of 5e, even though a different number of edge channels enters each of the voltage probes, these edge channels originate all from the same contact. Hence, the voltage probes float to the same electrochemical potential. For positive values of the magnetic field (top right panel), the region with filling factor ν_1 ($|\nu_1| < |\nu_2|$) can support fewer edge channels. The extra edge channels which exist in the region with filling factor ν_2 get reflected at the boundary (top right panel of 5e). After running along the junction they mix with channels originating from the other contact. From equation 2 we expect $h/3e^2 = 8604.269 \Omega$ which is in agreement with the observed value of 8535Ω . Also for the other combinations of integer quantum Hall states such as for instance (6,10) the edge channel picture with full equilibration performs very well. This is best seen in the horizontal and vertical line sections through the data of 5b plotted in panels c and d. Here, we find zero resistance for the negative sign of the field and $1.67 \text{ k}\Omega$ or close to $h/15e^2 = 1720.8538 \Omega$ for the positive sign.

In summary, we have investigated the influence of vacuum, elevated temperatures and some gases on the electronic properties of graphene. A hysteresis in the field effect behavior of graphene similar to what has been previously reported on carbon nanotubes, was observed under ambient conditions. It was attributed to adsorbed dipolar molecules such as water. Pristine graphene samples are typically p-type doped at a level of $2 \cdot 10^{12} \text{ cm}^{-2}$. Vacuum treatment reduces the hysteresis and also partially removes dopants. Additional

heat treatment under vacuum is more effective in removing the doping adsorbates. It also improves the sample homogeneity as attested by an increased value of the resistance at the charge neutrality point, which indicates an amplitude reduction of the electron-hole puddle landscape. Ammonia has served as an n-type dopant. It has been used to compensate the initial p-type doping without annealing. This chemical doping however leads to an enhanced inhomogeneity as reflected by a reduced resistance at the charge neutral point. An asymmetry between electron and hole mobilities can be observed. Finally, four terminal magneto-transport studies were performed on graphene p-n junctions fabricated by spatially selective chemical doping. These studies revealed a strong equilibration of edge channels near the junction.

References

- [1] K. S. Novoselov, A. K. Geim, S. V. Morozov, D. Jiang, Y. Zhang, S. V. Dubonos, I. V. Grigorieva, and A. A. Firsov. *Science*, 306:666, 2004.
- [2] F. Schedin, A. K. Geim, S. V. Morozov, E. W. Hill, P. Blake, M. I. Katsnelson, and K. S. Novoselov. *Nature Mater.*, 6:652, 2007.
- [3] B. Huard, J. A. Sulpizio, N. Stander, K. Todd, B. Yang, and D. Goldhaber-Gordon. *Phys. Rev. Lett.*, 98:236803, 2007.
- [4] B. Özyilmaz, P. Jarillo-Herrero, D. Efetov, and P. Kim. *Appl. Phys. Lett.*, 91:192107, 2007.
- [5] J. R. Williams, L. DiCarlo, and C. M. Marcus. *Science*, 317:638, 2007.
- [6] M. I. Katsnelson, K. S. Novoselov, and A. K. Geim. *Nature Phys.*, 2:620, 2006.
- [7] V. V. Cheianov, V. I. Falko, and B. L. Altshuler. *Science*, 315:1252, 2007.

- [8] P. Blake, E. W. Hill, A. H. Castro Neto, K. S. Novoselov, R. Jiang, R. Yang, T. J. Booth, and A. K. Geim. *Appl. Phys. Lett.*, 91:063124, 2007.
- [9] A. C. Ferrari, J. C. Meyer, V. Scardaci, C. Casiraghi, M. Lazzeri, F. Mauri, S. Piscanec, D. Jiang, K. S. Novoselov, S. Roth, and A. K. Geim. *Phys. Rev. Lett.*, 97:187401, 2006.
- [10] W. Kim, A. Javey, O. Vermesh, Q. Wang, Y. Li, and H. Dai. *Nano Lett.*, 3:193, 2003.
- [11] J. Martin, N. Akerman, G. Ulbricht, T. Lohmann, J. H. Smet, K. von Klitzing, and A. Yacoby. *Nature Phys.*, 4:144, 2008.
- [12] J. Moser, A. Verdaguer, D. Jimenez, A. Barreiro, and A. Bachtold. *Appl. Phys. Lett.*, 92:123507, 2008.
- [13] M. Ishigami, J. H. Chen, W. G. Cullen, M. S. Fuhrer, and E. D. Williams. *Nano Lett.*, 7:1643, 2007.
- [14] J. Moser, A. Barreiro, and A. Bachtold. *Appl. Phys. Lett.*, 91:163513, 2007.
- [15] V. V. Cheianov, V. I. Falko, B. L. Altshuler, and I. L. Aleiner. *Phys. Rev. Lett.*, 99:176801, 2007.
- [16] J. P. Robinson, H. Schomerus, L. Oroszlány, and V. I. Falko. *Phys. Rev. Lett.*, 101:196803, 2008.
- [17] B. Huard, N. Stander, J. A. Sulpizio, and D. Goldhaber-Gordon. *Phys. Rev. B*, 78:121402, 2008.
- [18] E. J. H. Lee, K. Balasubramanian, R. T. Weitz, M. Burghard, and K. Kern. *Nature Nanotech.*, 3:486, 2008.
- [19] K. S. Novoselov, A. K. Geim, S. V. Morozov, D. Jiang, M. I. Katsnelson, I. V. Grigorieva, S. V. Dubonos, and A. A. Firsov. *Nature*, 438:197–200, 2005.

[20] Y. B. Zhang, Y. W. Tan, H. L. Stormer, and P. Kim. *Nature*, 438:201–204, 2005.

[21] D. A. Abanin and L. S. Levitov. *Science*, 317:641, 2007.